KSCE Journal of Civil Engineering (2024) 28(12):5682-5696
DOI 10.1007/s12205-024-2550-x

pISSN 1226-7988, eISSN 1976-3808
www.springer.com/12205

Structural Engineering

Predicting FRP Plate End Debonding with a Neural Network Model Enhanced by Modified Sparrow Search Algorithm

Md. Ismail Monsury[a], **Nusrat Hoque**[a], **and Hasnat Rahman**[a]

[a]*Dept. of Civil Engineering, Chittagong University of Engineering & Technology, Raozan, Chittagong 4349, Bangladesh*

ARTICLE HISTORY

Received 9 January 2024
Revised 23 June 2024
Accepted 10 July 2024
Published Online 23 October 2024

KEYWORDS

Fiber reinforced polymer
Plate end debonding
Back propagation neural network
Quantum-computations and multi-strategy enhanced sparrow search algorithm

ABSTRACT

Fiber Reinforced Polymer (FRP) plates are widely used to strengthen structural members, but their potential is limited by plate end debonding failure. Existing models that are developed to address plate end debonding failure considered only few parameters and primarily based on fracture mechanics or shear strength of beams. Following study aims to develop a Back Propagation Neural Network (BPNN) model optimized by a quantum-computations and multi-strategy enhanced Sparrow Search Algorithm (QMESSA) to effectively forecast the plate end debonding load of externally bonded FRP plates. Where the model utilized complex nonlinear relationship between all the prominent governing parameters and the debonding load. Optimization accuracy and generalization is hindered by local minima problem in BPNN. Incorporating QMESSA significantly reduced the local minima problem in BPNN substantiated by an increased testing data sets regression value from 0.82 to 0.98. Reliability analysis showed that the model outperformed the existing international codes and shear-based model in terms of accuracy and stability. Results from the correlation analysis of parameters revealed that the web reinforcement ratio is the most influential parameter for debonding prediction. Therefore, QMESSA optimized BPNN model can be used as an effective tool for designing FRP to prevent FRP plate end debonding.

1. Introduction

Reinforced concrete deteriorates over time due to various reasons, such as corrosion of internal reinforcement, freeze-thaw action, chemical attack, overloading and poor construction quality. It is considered to be more environmentally and economically preferable to retrofit structures rather than rebuilding. Retrofitting with steel plates on the tension face of a structural member is often utilized, but this method has significant drawbacks, primarily due to issues with corrosion. The use of fiber reinforced polymers (FRPs) for the repair and restoration of existing reinforced concrete structures is becoming more and more common (Biscaia, 2001; Sen, 2015). Advantages such as lightweight, corrosion resistance, high tensile strength, reduction of concrete strain, design flexibility are highly desirable (Hollaway, 2010; Kotynia et al., 2021). Scientists conducted a range of experiments to investigate the flexural performance of reinforced concrete (RC) beams that had been strengthened using FRP systems. A study found that beams that have a low reinforcement ratio, bonding thin FRP plates to the tension face significantly enhances the flexural strength of beams (Deng, 2001). However, strengthening reinforced concrete with FRP can lead to brittle failure by the plate separating from the beam prematurely and unpredictably at relatively low magnitude of load relative compared to its high rupture strength (Chen and Teng, 2003). This phenomenon greatly limits the use of FRP in practical fields. The debonding of FRP plate can be classified as (a) Intermediate crack (IC) debonding: Starts at the midspan where flexural stress is high and moves towards plate end; (b) Plate End (PE) Debonding: starts at the plate end by high interfacial stress and propagates away from plate end towards midspan (Aram et al., 2008; Narayanamurthy et al., 2012).

Various computational models have been developed by researchers to address the issue of debonding at plate end. Primary focuses are on factors such as the shear force exerted on concrete beams as well as the value of strain at which debonding occurs in the FRP.

CORRESPONDENCE Nusrat Hoque nusrat_hoque@cuet.ac.bd Dept. of Civil Engineering, Chittagong University of Engineering & Technology, Raozan, Chittagong 4349, Bangladesh

Oehlers strength model showed the calculation of PE debonding by considering the combined effect of shear forces and flexural forces (John, 1992). A model based on only concrete shear strength was proposed by Smith and Teng (2002). PE debonding occurs in beams having a comparatively low shear span to depth ratio (John, 1992; Smith and Teng, 2002). PE debonding phenomenon emerges in beams where the bending moment is relatively low, leading to shear becoming the dominant factor governing their behaviour instead of flexure (Lau et al., 2001). Jansze proposal for the strength model of PE debonding, examined the occurrence of PE debonding failure at shear crack initiation of RC beams (Jansze, 1997). Majority of models rely either on beams shear strength or the principles derived from fracture mechanics. An empirical shear-based formula was presented by Ahmed et-al which is based on available literatures on FRP PE debonding models. Model is developed upon beams concrete shear strength by accounting for the governing parameters initializing shear cracks (El-Sayed et al., 2021). Finite element analysis had been put forward in order to understand the intricate relationship among the governing parameters of debonding failure (Al-Saawani et al., 2022). Despite the complex relationship between PE debonding and governing parameters of FRP-strengthened RC beams addressed, existing models often exhibit appalling robustness and moderate computation accuracy. Hence, there requires a crucial step to develop a more accurate relationship between debonding of PE and every individual parameter. Despite several research studies, the mechanisms underlying this type of failure are intricate and not yet fully comprehended. Because of this, the majority of design guidelines and codes advise taking particular precautions to prevent PE debonding. For example, extending the length of the FRP plate beyond a certain point does not enhance the bonding strength (Chen and Teng, 2001). Many design codes and guidelines emphasize the importance of anchorage methods at terminating point of FRP plate for prevention of PE debonding (Al-Saawani et al., 2015, 2023; 440, 2017; Eslami et al., 2019). However, to improve the design of end-anchorage mechanism, crucial step is to initially ascertain the shear force at which PE debonding takes place. Hence, it is necessary to find effective solutions that can either prevent or delay debonding failures, or utmost utilization of FRP before failure.

At present, Machine Learning is becoming an emerging field in the contemporary research world. Köroglu proposed an BPNN model and concluded that if the intricate connection between the bond strength of FRP bars in concrete and the factors influencing this bond strength has been identified, model could serve as a promising alternative to conventional statistical and experimental approaches (Köroglu, 2019). Abuodeh explored the use of Machine Learning techniques to identify the behaviour of RC beams strengthened with FRP laminates (Abuodeh et al., 2020). BPNN possesses inherent capabilities for nonlinear mapping and offers improved simulation of complex nonlinear relationships (Yu et al., 2008; Ma et al., 2021).

Nevertheless, while the gradient descent optimizer is used to determine weights and biases in the BPNN, it has limitations. It can often result in the model getting trapped in local optima problem and slow convergence speed (Choi et al., 2008). Hence, there is a need for improvement through the utilization of better algorithms. Besides, due to small datasets availability for training a machine learning model, it becomes less effective in prediction accuracy. Scientists are pondering on how to find an optimal solution to this small data sets problem. From the time being, optimization algorithm has been used in BP neural network to enhance performance and achieve optimality. In 2020, a novel optimization algorithm namely Sparrow Search Algorithm (SSA) was put forward (Xue and Shen, 2020). This algorithm is used in BPNN to overcome local minima issues in prediction models. To improve prediction accuracy for calculating debonding strain in FRP strengthened beams, a BPNN model was constructed and further optimized using SSA (Li et al., 2021), illustrating the potential effect of SSA algorithm in optimization problems. However, SSA algorithm has some drawbacks in terms of its poor optimization accuracy and scanty efficiency in search technique. For example. the SSA algorithms' optimization performance is hindered by shortcomings in the quality of the initial population generation and an imbalance between exploration and exploitation abilities. This imbalance results in slow convergence and leads the algorithm to get trapped in local optima, resulting in poor optimization accuracy. Several techniques and approaches are taken in scholarly articles to ameliorate the shortcomings of SSA algorithm. An improved SSA based on quantum computations and multi-strategy enhancement (QMESSA) which showed excellent results in accuracy and convergence of the algorithm was put forward (Wu et al., 2023).

Addressing the aforementioned limitations, this study focuses on constructing an optimal prediction model using a BPNN with enhanced generalization capability and high prediction accuracy. A dataset consisting of 128 samples with 13 parameters is used for training, validation and testing the BPNN model as well as QMESSA optimized BPNN model. The model accounts for all the governing parameters that affects the plate end debonding of FRP. The proposed model aimed to mitigate the issue of local minima by incorporating the QMESSA in the BPNN. QMESSA is utilized as weights and biases optimization technique in BPNN. The outcomes of this study are expected to provide valuable information on how the proposed model predicts PE debonding load efficiently by developing a complex non-linear relationship among the governing failure parameters and debonding load.

The following characteristics distinguish this paper from previous works:

1. A detailed and comprehensive neural network model is proposed including the effects of all parameters related to plate end debonding.
2. The model incorporates Quantum-computations and Multi-strategy Enhanced Sparrow Search Algorithm (QMESSA) to mitigate the local minima problem in the optimization process of back propagation neural network model.
3. QMESSA optimized BPNN model addressed the generalization issue with the help of optimal sets of initial

weights and biases indicating that, the current model is much effective in terms of prediction accuracy.

4. A detailed parametric study has been carried out to identify the most influential parameter effecting the plate end debonding.

Remaining structure of this article is outlined as follows. Section 2 demonstrates how BPNN works followed by the introduction and display of QMESSA. In section 3 a description of data set collection and parameter identification for training and testing the model is delineated. Section 4 presents how the proposed model has been designed. In section 5, results and discussion of the model is substantiated. Section 6 describes the model reliability analysis with comparison to existing codes and the shear-based model to showcase the robustness of the model and substantiated the importance of proposed model in the design process of FRP strengthened RC beams. In section 7, correlation analysis of parameter is conducted in order to identify the most influential parameter affecting PE debonding. Finally, in section 8 conclusions are drawn based on the result and comparison of the model.

2. Back Propagation Neural Network and Modified Sparrow Search Algorithm

2.1 Back Propagation Neural Network (BPNN)

The BPNN is a typical feed forward neural network with multiple layers, consisting of the input layer, hidden layer, and output layer. It is trained using the error backpropagation algorithm and employs the weight and threshold adjusting method by means of gradient descent for each neuron in each layer. The primary objective is to reduce errors in the network output until they achieve a predetermined level of convergence prior to completing the full training of the network. The BPNN is capable of nonlinear aligning between input and target, and possesses self-instructed abilities with a straightforward structure. However, a drawback of the BPNN is its susceptibility to getting stuck in local minima, resulting in poor stability (Bianchini et al., 1994). The fundamental composition of the BPNN is depicted in Fig. 1.

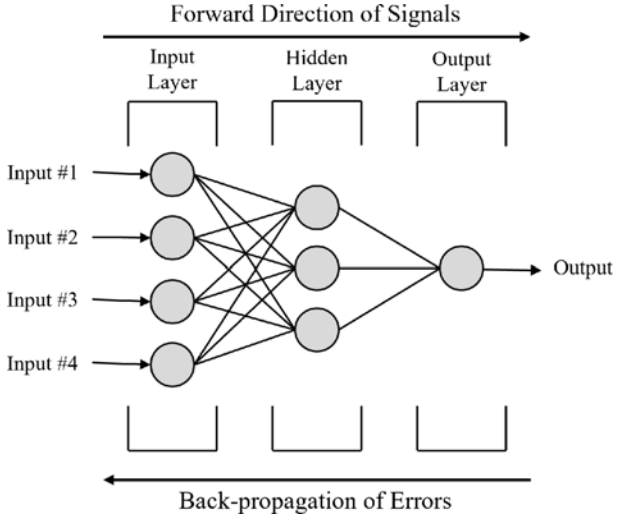

Fig. 1. Backpropagation Neural Network (BPNN) Architecture

2.2 Modified Sparrow Search Algorithm

Quantum computations and multi-strategy enhancement of sparrow search algorithm (QMESSA) is a unique updated swarm intelligence optimization technique. Features of QMESSA algorithm is given below:

1. Initial population generation with more randomization and diversity by employing circle chaotic mapping combining quantum computations and quantum gate mutations.
2. An adaptive T-distribution to help the algorithm jump out of local minima.
3. A precision elimination strategy to help creating a balance between exploration and exploitation of the algorithm.

Properties of QMESSA help SSA to converge first, avoid the local minima, and increase the efficiency and accuracy. Procedural steps of QMESSA are illustrated in Fig. 2.

Mathematical formulation of QMESSA is demonstrated below:

Step 1: First, formulation of initial population of sparrows is conducted. To enhance the initial population quality of sparrows, varied starting population approach method was suggested which includes improved circle chaotic mapping and quantum theory. The first step involves initializing the population using an improved circle chaotic mapping technique. The equation follows:

$$y_{i+1} = mod\left(y_i + 0.4204 - \left(\frac{0.0305}{\pi}\right)\sin(2\pi y_i), 1\right), \tag{1}$$

$$x_{i,j} = lb + (ub - lb) \times y_i, \tag{2}$$

where $x_{i,j}$ is a matrix which denote the position of sparrows in search space, y_{i+1} is the expression of circle chaotic mapping, *up* (upper bounds) and *lb* (lower bounds) states the limits or boundaries of the exploration space. Next step is, during the initialization stage, integration of quantum computing principles was considered, enabling the generation of additional initial populations using a collection of qubits. Suppose the position that has been developed by Eq. (1) in terms of sine (x_s) or cosine location (x_c), then angle of rotation (θ) can be developed from the following equation:

$$\theta = arcsin\left(\frac{2(x_s - lb)}{ub - lb} - 1\right), \tag{3}$$

$$\theta = arccos\left(\frac{2(x_c - lb)}{ub - lb} - 1\right). \tag{4}$$

Further, some new population position can be deduced by the following equation:

$$x_s = \frac{1}{2}((\sin\theta + 1)(ub - lb)) + lb, \tag{5}$$

$$x_c = \frac{1}{2}((\cos\theta + 1)(ub - lb)) + lb. \tag{6}$$

Added that, to diversify initial population, dynamic quantum

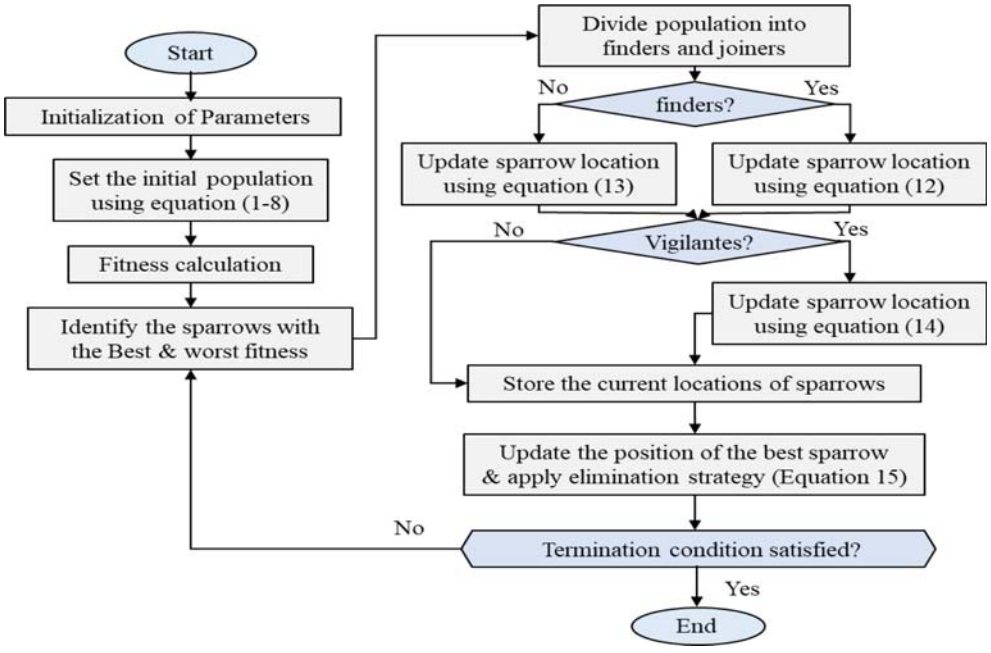

Fig. 2. Flow Chart of QMESSA Algorithm

rotation gate mutation was considered by the following equation:

$$R(\theta_r) = \begin{bmatrix} \cos\theta_r & -\sin\theta_r \\ \cos\theta_r & \sin\theta_r \end{bmatrix}, \tag{7}$$

here, $\frac{\pi}{4} \le \theta_r \le \frac{\pi}{2}$. The updating process is follows:

$$\begin{bmatrix} \cos\theta' \\ \sin\theta' \end{bmatrix} = R(\theta_r) \begin{bmatrix} \cos\theta \\ \sin\theta \end{bmatrix}. \tag{8}$$

Following a mutation induced by a rotation gate, individual positions in a population are determined using Eqs. (1), (5), and (6). The initial population is then compared to the mutated population, and individuals with superior sine and cosine positions are chosen for the final initial population.

Step 2: The fitness values of individuals in the final initial population are computed. The positions of the best and worst-performing sparrows are sorted based on fitness. The finder, representing the sparrow initiating the search for food, possesses the highest fitness and acts as the primary explorer for the group, communicating food source locations to joiners. Finders, with a broader search capability, play a pivotal role in the exploration process compared to joiners. The location update formula of finders, joiners, and vigilantes to search for food is given in the literature (Xue and Shen, 2020). The algorithm employs an adaptable T-distribution factor in the location update formulas of finders, joiners, and vigilantes to enhance search strategy. This factor promotes exploratory phases in initial iterations, aiding in escaping local optima. As iterations progress, the mutation factor gradually shifts focus towards exploitation, maintaining a balance between exploration and exploitation. This prevents premature confinement to local optima, ensuring accelerated convergence in later stages. The adaptive T-distribution variation factor is given below:

$$T = T\left(\frac{a^t}{m}\right) = T\left(\frac{1}{m} \times \exp\left(\frac{\ln(t_c)^t}{t_c}\right)\right), \tag{9}$$

$$a = \exp\left(\frac{\ln(t_c)}{t_c}\right), \tag{10}$$

$$t_c = \frac{iter_{max}}{5}. \tag{11}$$

Here, t denotes the present iteration, $iter_{max}$ states iterations of maximum number, t_c is a critical point at the time of iteration process, a is a value which depends on t_c, m is a scaling factor which is taken as a value of 10.

Hence, the enhanced strategy was implemented to facilitate iterative updating, corresponding location update formulas of finders, joiners, and vigilantes are as follows:

Following the equation of a finder to update position:

$$X_{i,j}^{t+1} = \begin{cases} X_{i,j}^t \cdot \left(\tau \exp\left(-\frac{i\mu}{\alpha \cdot iter_{max}}\right) \cdot (2r_1 - 1) \cdot \sqrt{r_2} + (r_3 - 0.5)^5\right) \\ \qquad \text{if } (R_2 < ST) \\ X_{i,j}^t + T\left(\frac{1}{m} \times \exp\left(\frac{\ln(t_c)}{t_c}\right)^t\right) \cdot L \qquad if \;\; R_2 \ge ST. \end{cases} \tag{12}$$

$X_{i,j}$ denotes sparrow location details in the j[th] dimension. Additionally, the algorithm uses α, a randomly chosen number ranging in between 0 to 1, R_2, a preliminary alert threshold lies in between 0 and 1, ST, a safety threshold value between 0.5 and 1, and L, a $1 \times d$ matrix comprising entirely of elements equal to 1. When R_2, > ST, indicates the absence of nearby predators, allowing the sparrow to explore its surroundings extensively. However, if

$R_2 \leq$ ST, all sparrows must look for safe locations to forage. τ and μ are random constants ranges from [1.5, 2.5] and [4, 12] respectively, r_1, r_2, r_3 are random numbers within the range of 0 to 1.

Next, the position update of a joiner is as follows:

$$X_{i,j}^{t+1} = \begin{cases} T\left(\frac{1}{m} \times \exp\left(\frac{\ln(t_c)}{t_c}\right)^t\right) \cdot \exp\left(\frac{x_{worst}^t - x_{i,j}^t}{i^2}\right) & if\ i > n/2 \\ X_p^{t+1} + \left|X_{i,j}^t - X_p^{t+1}\right| \cdot A^+ \cdot L & otherwise, \end{cases} \quad (13)$$

where X_p states the optimal location where finder is positioned, X_{worst} indicates present global worst position, A is a matrix consisting of a single row and d columns.

Position update formula of a vigilante given below:

$$X_{i,j}^{t+1} = \begin{cases} X_{best}^t + T\left(\frac{1}{m} \times \exp\left(\frac{\ln(t_c)}{t_c}\right)^t\right) \cdot \left|X_{i,j}^t - X_{best}^t\right| & if\ f_i > f_g \\ X_p^t + K \cdot \left(\frac{\left|X_{i,j}^t - x_{worst}^t\right|}{(f_i - f_w) + \varepsilon}\right) & if\ f_i = f_g, \end{cases} \quad (14)$$

where X_{best} is optimal current global position. K falls randomly within the range of -1 to 1. f_i represents a single sparrow fitness at present, while f_w and f_g indicate the worst fitness value and current global optimum fitness, respectively. Additionally, ε is a small constant. If $f_i > f_g$, then the sparrows are in a precarious position near the population boundary and are at risk of being attacked. If $f_i = f_g$, sparrows occupy a central position within the population and need to seek safety by flying towards other sparrows.

Step 3: Individuals with the lowest fitness scores are removed after a series of iterations. A strategy for precise elimination is implemented, generating new individuals to replace them, outlined as follows:

$$X_{i,j}^{t+1} = X_{best}^t + (ub - lb) \times R_r \times T\left(\frac{1}{m} \times \exp\left(\frac{\ln(t_c)}{t_c}\right)^t\right), \quad (15)$$

$$R_r = 1 - \frac{t}{iter_{max}}, \quad (16)$$

where ub and lb states the upper and lower bounds of search space, R_r indicates the dynamic radius of search space. Rest meanings of the symbol in the formula remains same as above.

Step 4: A novel boundary control approach is proposed, utilizing the positional data of optimal and suboptimal individuals to regulate the search boundary. This can be expressed as:

$$X_{i,j}^{t+1} = X_{best2}^t + r \times (X_{best}^t - X_{best2}^t), \quad (17)$$

where X_{best2}^t and X_{best2}^t refer to the globally optimal and globally suboptimal results in i^{th} iteration, respectively, r is randomly chosen number ranged in between [0,1]. The approach randomly places individuals outside the specified boundary near those with higher fitness. In successive iterations, these individuals explore their surroundings using improved positions, enhancing SSAs exploitation capability.

Step 5: The algorithm seeks the current optimal value by comparing it to the previous generation optimal value. If the current value surpasses the previous one, the algorithm updates the finest value. It iterates until the criterion is met, ultimately identifying the globally best fitness value and its location.

3. Description of Experimental Data and Parameter Identification

For training and validation of a neural network, a substantial amount of data is required. An extensive literature review was carried out to create a comprehensive dataset of experimental test results on reinforced concrete (RC) beams strengthened with FRP plates, which eventually fail in plate end debonding. 128 experimental test results are collected from the article (El-Sayed et al., 2021) for building the neural network model. The database consists of 114 beams tested with four-point bending systems and 14 beams tested with three-point bending systems. Beams that are included in the database, had to meet specific criteria that follows: a) failure had to occur through PE debonding, either by interfacial debonding or CCS.; b) every specimen were rectangular sections of conventionally reinforced beams with simple support; c) the FRP were not under any anchorage system; d) beams were tested using either a three-point or four-point bending system.

The beams have a wide range of geometric properties. From Fig. 3, we can get that the test beams varied in width from 100 – 400 mm and has a height range of 100 – 450 mm. Clear span length is in between 812 – 3,800 mm, and the shear span/depth ratios varied from 2.29 – 6.25. Steel Continued reinforcement ratio in the tension zone was between 0.32% and 2.12%. Material properties also showed a wide range. Some beams (43) were strengthened with pultruded plates of FRP, while others were reinforced with FRP sheets of wet lay-up. FRP width varied from 30 – 360 mm. Thickness of dry fibers for wet lay-up FRP sheets ranged in between 0.11 – 0.176 mm. Pultruded FRP plates total thickness is in between 0.82 – 4.76 mm. Modulus of elasticity of FRP materials ranged from 10.3 – 400 GPa. The ratio of the length of the plated section beyond the point load to the shear span of the beam ranged from 0.25 – 1.00. Additionally, beams compressive strength varied from 19.2 – 66.4 MPa.

4. Model Design

The parameters affecting the plate end debonding most are considered for designing the model. Model design and simulation works were conducted using MATLAB (2018) programming language. Design of BPNN model and how the QMESSA algorithm has been implemented in BPNN model for predicting plate end debonding load are explained as follows:

1. Thirteen input parameters are considered as input layer of the designed BPNN. As a result, there are thirteen input neurons in input layer of BPNN. They are–width (b), depth (d), compressive strength (f_c'). Then, properties of steel reinforcement – yield strength (f_y), shear reinforcement (f_{yv}), shear reinforcement ratio (ρ_{sv}), FRP reinforcement property – modulus of elasticity (E_{frp}), ultimate strength (f_{fu}), thickness

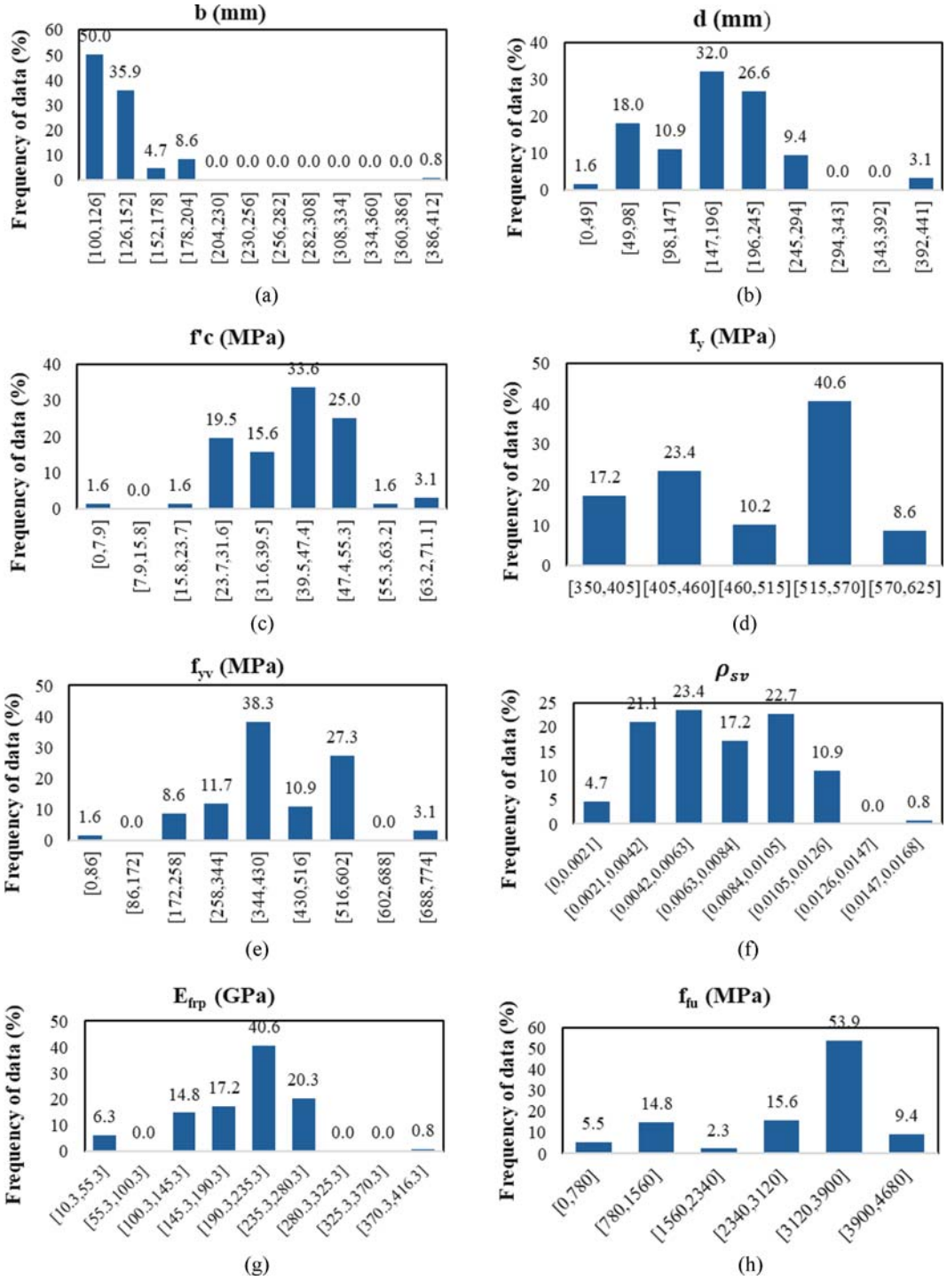

Fig. 3. Range of the Parameters: (a) b, (b) d, (c) f_c' , (d) f_y, (e) f_{yv}, (f) ρ_{sv}, (g) E_{frp}, (h) f_{fu}

(t_{frp}), width (b_{frp}), Loading configuration – clear span of beam (L), shear span (a), FRP curtailment length (L_{up}).

2. One output layer with one hidden neuron is used for the debonding failure load ($P_{u,exp}$).
3. One hidden layer is used in BPNN. Number of hidden neurons is determined through an empirical equation:

$$L = \sqrt{m+n} + a \,. \tag{18}$$

4. Here, L is the hidden neurons number in hidden layer; m is input layer neurons number; n is neuron in output layer; 'a' is a number taken in between 1 to 10. With a number of trials and considering overfitting and underfitting problem L is selected as 10. A topology is drawn in the Fig. 4. Dimensions (d) of BPNN that need to be optimized by QMESSA is calculated by the following equation:

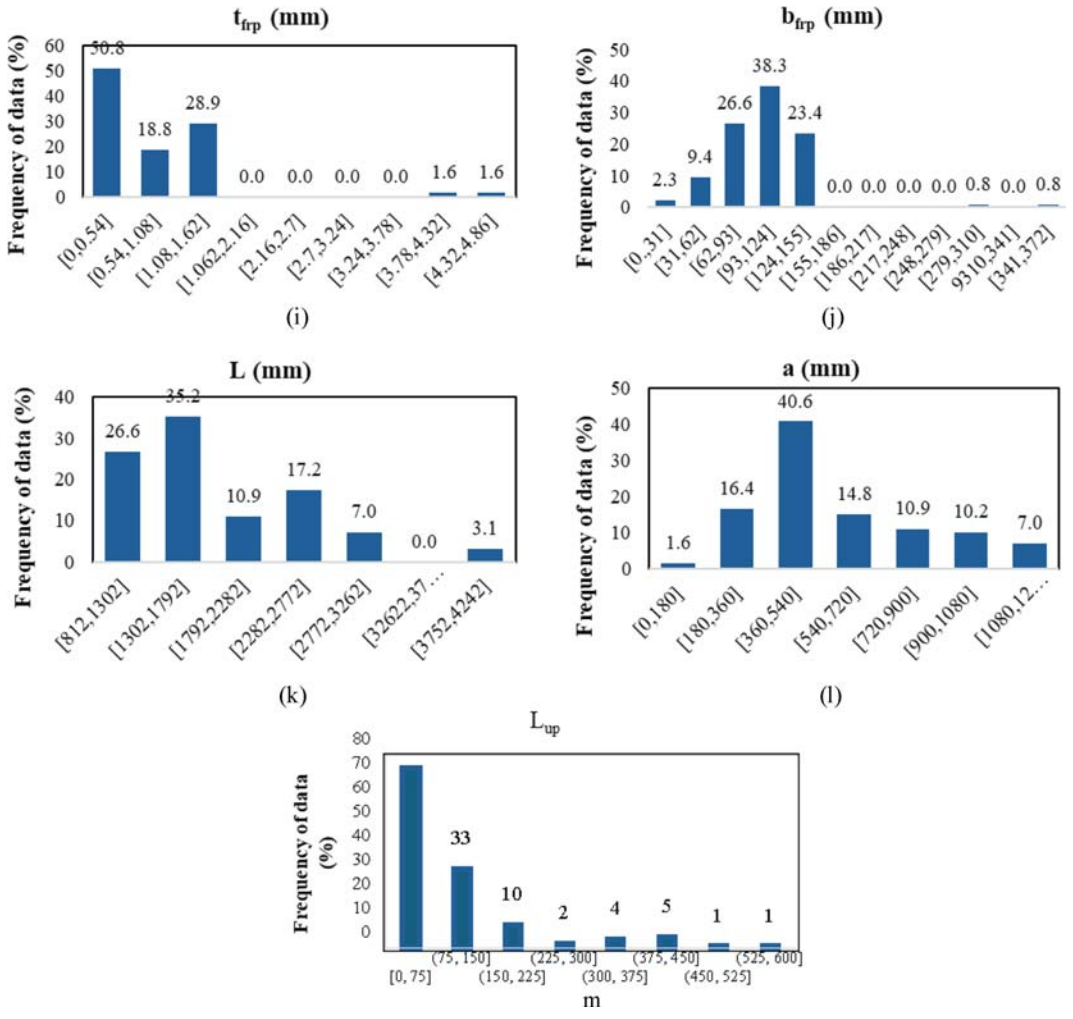

Fig. 3. (continued): (h) f_{fu}, (i) t_{frp}, (j) b_{frp}, (k) L, (l) a, (m) L_{up}

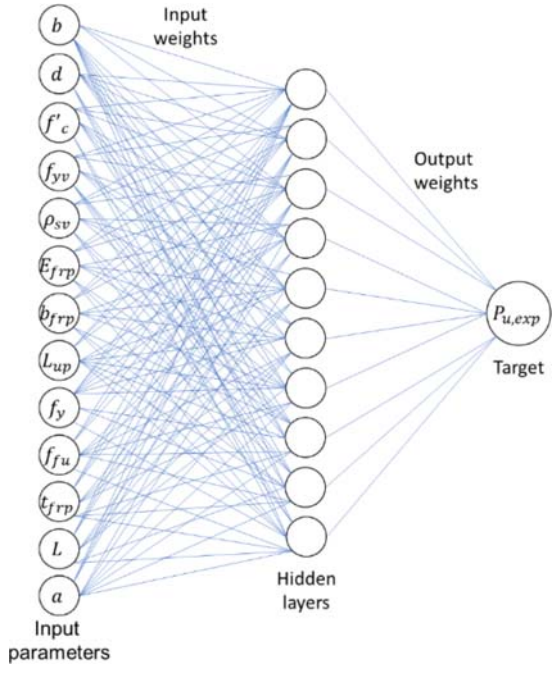

Fig. 4. Topology of the Designed Model

Table 1. Parameter Initialization of QMESSA-BPNN Model

Parameter	Value	Description
Size of population	70	-
Primary location	[-2,2]	Originated arbitrarily
Finders number	20%	-
Safety threshold	0.8	-
Dimension of sparrow	151	-
Upper and lower limits of Sparrow position	-2 ~ 2	-
Maximum iterations of QMESSA	500	-

$$d = u \times v + v + v \times w + w\,, \tag{19}$$

where u is input neurons number, v is hidden neurons number, and w is output neuron number. Here, d means the total weights and biases of the BPNN. QMESSA algorithm has been utilized to optimize these weights and biases of BPNN. Next, with the help of optimized weights and biases BPNN starts the training process.

Parameters of the QMESSA are initialized. For the purpose of applying the QMESSA algorithm in BPNN, values of

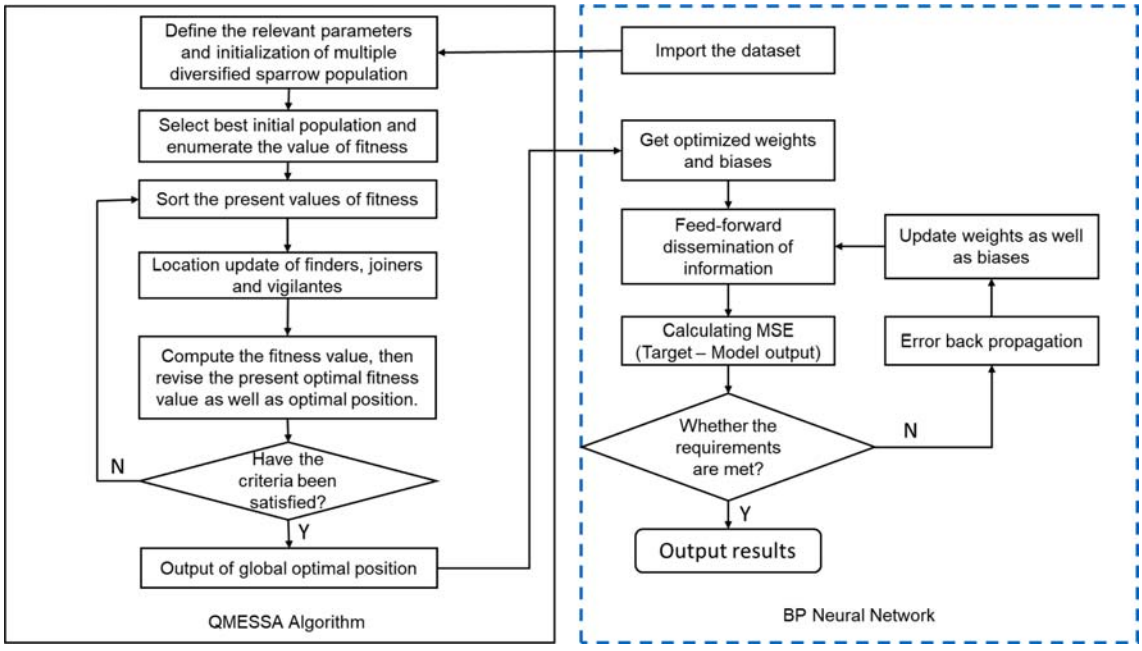

Fig. 5. Flow Diagram of QMESSA Optimized BPNN Model

different parameters are given in the Table 1. How the QMESSA algorithm is implemented in the BPNN is illustrated clearly in Fig. 5.

5. In the QMESSA algorithm function of fitness is shown in equation 20 and it can be used to measure population fitness by recording the optimal fitness value as well as optimal position globally, ranking the fitness values, updating the positions of finders, joiners, vigilantes, and calculating each of their fitness values separately. An individual fitness value improves with decreasing fitness value.

$$Fitness = \sum_{i=1}^{n} |y_i - \hat{y}_i| \tag{20}$$

Here y_i is the target output and $\hat{y}_i$ is the predicted output.

6. Update sparrow position by means of current fitness value if a value lower than the present fitness value emerges.
7. When the value of fitness is at its lowest point or has gone through all possible iterations, optimization is said to be complete. If not, go back to step *V*.
8. The BPNN weights and biases are given the sparrow position with the lowest value of fitness, allowing the best weights and biases to be obtained. After that, training process of BPNN starts.
9. For training the neural network 'trainlm' training function is applied in the network. LM of 'trainlm' training function stands for Levenberg-Marquardt algorithm. Properties of training parameters are given in the Table 2.
10. 128 experimental samples as stated in previous section are randomly divided into training (70%), validation (15%), and testing (15%) sets for neural network analysis.
11. For evaluating model generalization ability and prediction accuracy, mean squared error (MSE) and perfection to fit (Regression- 'R') are calculated and compared.

$$MSE = \frac{1}{n}\sum_{i=1}^{n}(z_i - \hat{z}_i)^2 \tag{21}$$

Here z_i is the target output and $\hat{z}_i$ is the predicted output from the model. Target output is the experimental value (debonding failure load). Predicted output is what the QMESSA-BPNN model is predicting (debonding failure load). MSE is calculated and minimized at each iteration of BPNN until it reaches to a specified value as declared.

Table 2. Properties of Training Parameters

Training Parameters	Property
Training function	'trainlm'
Activation function (hidden layer)	'tansig'
Activation function (output layer)	'purelin'
Maximum epoch	1000
Learning rate	0.01
Maximum validation check	6
Performance (MSE) goal	0
Minimum Gradient	1e-07

5. Results & Discussions

The graphical representations provided in Figs. 6 and 8, clearly illustrate that the QMESSA optimized BPNN model achieves higher regression coefficient values compared to the BPNN model across the training, validation, and testing datasets. Specifically, the QMESSA-BPNN model demonstrates regression coefficients of 0.994, 0.996, and 0.985, while the BPNN model yields regression coefficients of 0.997, 0.977, and 0.817 for the respective datasets.

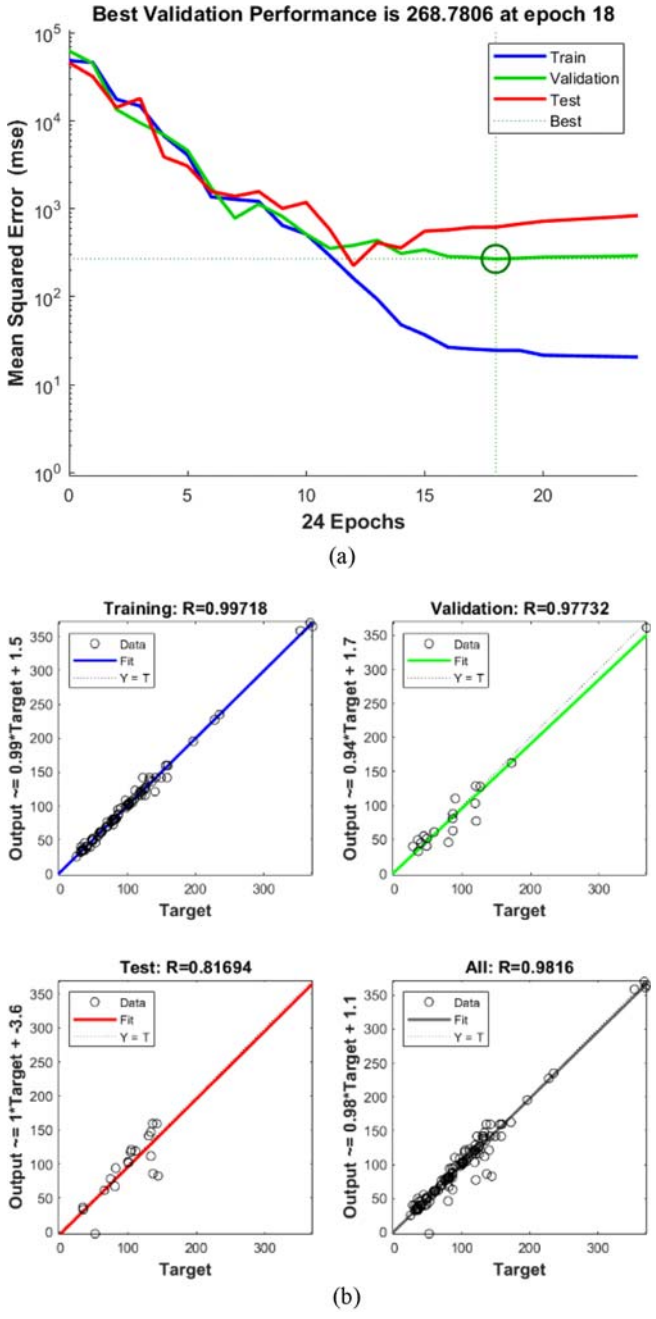

Fig. 6. Result of BPNN Model: (a) Performance, (b) Regression

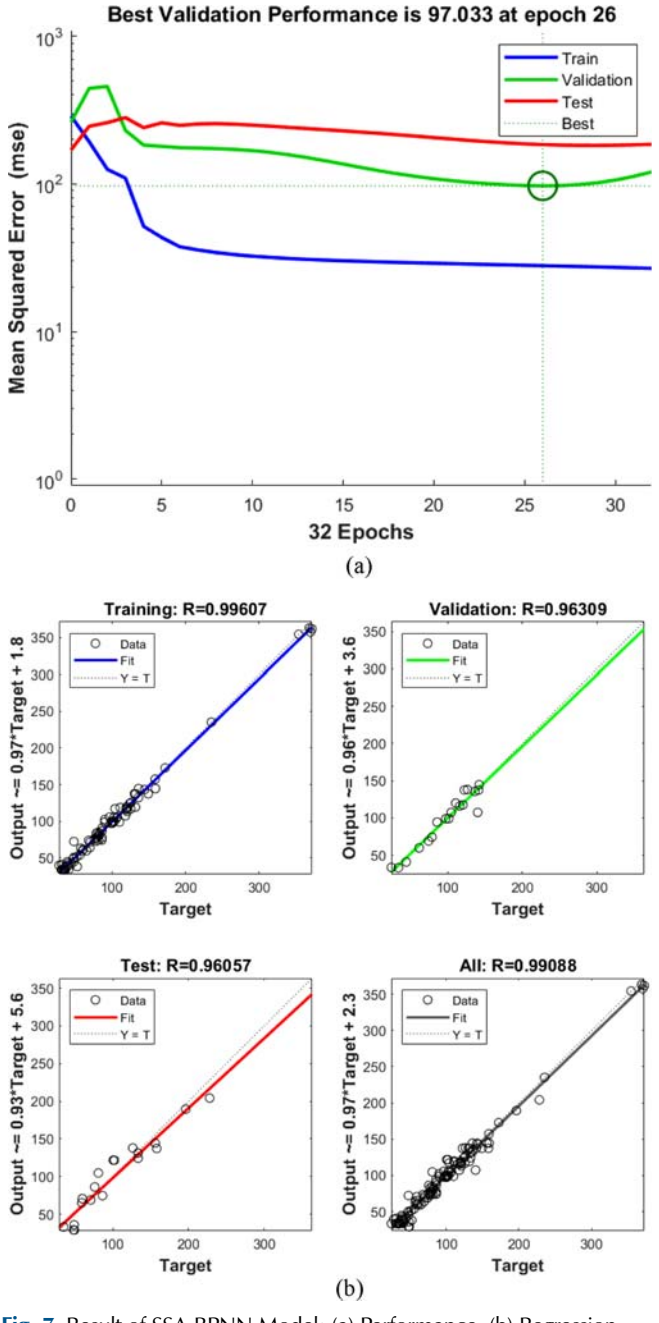

Fig. 7. Result of SSA-BPNN Model: (a) Performance, (b) Regression

Besides, in Fig. 9 it is seen that MSE is significantly reduced in test data set for the QMESSA-BPNN model (230.42) with respect to BPNN model (512.53), illustrating the enhanced accuracy of the model. It is noteworthy that both models exhibit satisfactory performance on the training set in terms of regression value on training stage. However, the BPNN model exhibits an overfitting issue, as evidenced by the substantially lower regression coefficient on the test data. This occurrence can be attributed to the extensive training of the BPNN model, leading to an overly complex model that hinders to generalize effectively beyond the training data. It is evident that the BPNN model exhibits substantially higher deviation in predicting result from experimental result in both the validation and test datasets compared to the QMESSA-BPNN model. Another reason is because of local minima problem during the training process. To explain broadly, the optimization algorithm ('trainlm') failed to reach the global minima.

A comparison among the models is given in the Table 3.

Consequently, the inability of BPNN model to accurately predict output when provided with new sets of data is clearly seen. In contrast, the QMESSA-BPNN model successfully resolves the overfitting issue, as indicated by its higher regression coefficient value of 0.985 in the test datasets. In addition, the dynamic property of QMESSA helped to achieve a higher regression result on test dataset as compared to SSA. SSA-BPNN model achieved a

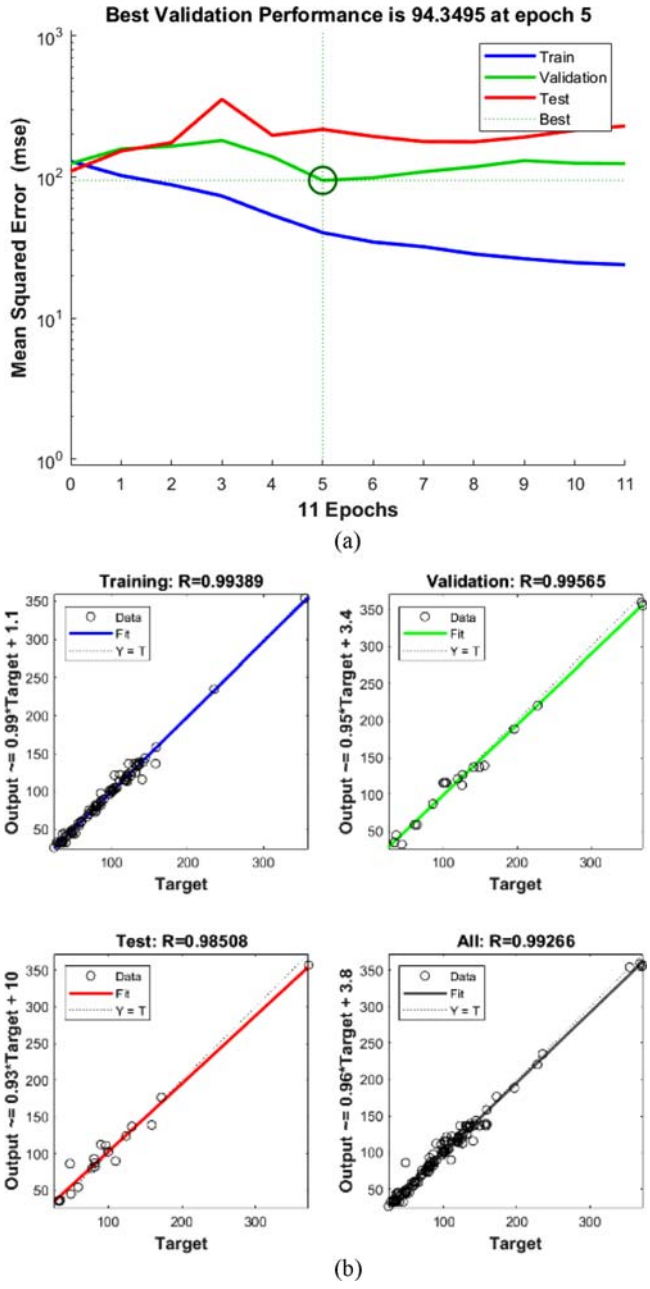

Fig. 8. Result of QMESSA-BPNN Model: (a) Performance, (b) Regression

regression score of 0.96 on test datasets as shown in Fig. 7. Besides, QMESSA-BPNN model converges within 5 epochs compared to SSA-BPNN model (26 epochs). Reasons for these phenomena are because of initial quality population of sparrows ensured by chaotic mapping and quantum computations, enhanced

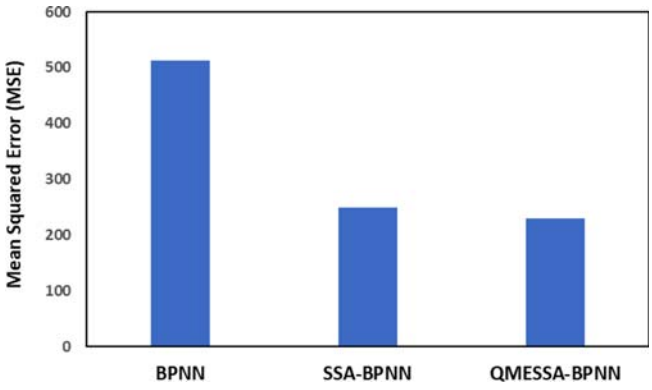

Fig. 9. Performance of the Models (MSE)

search strategy of sparrows which accomplished to increase the exploration and exploitation ability of the algorithm, elimination strategy to accelerate the convergence. All these dynamic adaptability power of quantum mechanics and multiple strategy incorporated in SSA helped it to further jump out of the local minima, optimized the search space, and increased the generalization ability while being implemented in BPNN. As a result, the QMESSA-BPNN model demonstrates considerable improvement in terms of its generalization ability and prediction accuracy. Finally, results from above emphasize the superior performance of the QMESSA-BPNN model with its ability to generalization, providing a distinct advantage over the SSA-BPNN, and BPNN model. The reason that all the models achieved high MSE is because of extreme outliers' presence in datasets. As a result, summation of squared error increases.

6. Reliability Evaluation of Codes

Numerous models had been developed to forecast the occurrence of debonding failure at PE in RC beams strengthened with FRPs. The models primarily rely either on fracture mechanics principles or shear strength of beams. To conduct a comprehensive analysis of the efficacy of the QMESSA-BPNN model, a comparison was made between the QMESSA-BPNN model and various existing international codes as well as with a shear-based model. After performing the training and validation of the QMESSA-BPNN model an object of the model has been created in the workspace of MATLAB. Using the model object, debonding load is calculated by giving the input values of 13 parameters in the model object. In addition, it only takes the value of 13 input parameters (described in section 3) to predict the output debonding load from the model object.

Table 3. Comparison among BPNN, SSA-BPNN, and QMESSA-BPNN Models

Comparison among Models	Regression			Best Validation Performance (MSE)	Test Dataset Performance (MSE)
	Training	Validation	Testing		
BPNN	0.99718	0.97732	0.81694	268.78	512.53
SSA-BPNN	0.99607	0.96309	0.96057	97.03	248.58
QMESSA-BPNN	0.99389	0.99565	0.98508	94.35	230.42

In 2020 an empirical shear-based formula was put forward for prediction of debonding failure at PE for FRP beams, based on the existing models available in the literature and factors governing the debonding failure criteria (El-Sayed et al., 2021). The proposed shear force at PE region that initiates debonding can be expressed as:

$$V_{db,end} = \beta_v \beta_L 2.17 \left(f_c' \rho_{eq} \frac{d_{eq}}{a} \right)^{1/3} b d_{eq} . \quad (22)$$

β_v is a factor for shear reinforcement ratio (ρ_v). This is expressed in:

$$\beta_v = 2.15(\rho_v)^{0.06} . \quad (23)$$

β_L is a factor that accounts for the influence of ratio of the FRPs unplated length (L_{up}) to the beams shear span (a). The equation follows:

$$\beta_L = 0.57 \left(\frac{L_{up}}{a} \right)^{-0.34} \leq 1.0 . \quad (24)$$

d_{eq} is the equivalent effective depth expressed as:

$$d_{eq} = \frac{A_s E_s d + A_{frp} E_{frp} h}{A_s E_s + A_{frp} E_{frp}} . \quad (25)$$

ρ_{eq} is the equivalent reinforcement ratio stated as:

$$\rho_{eq} = \frac{\left(A_s + A_{frp} \frac{E_{frp}}{E_s} \right)}{(b d_{eq})} , \quad (26)$$

where f_c' is the compressive strength of concrete; a is denoted as shear span; E_s and A_s are the internal modulus of elasticity and

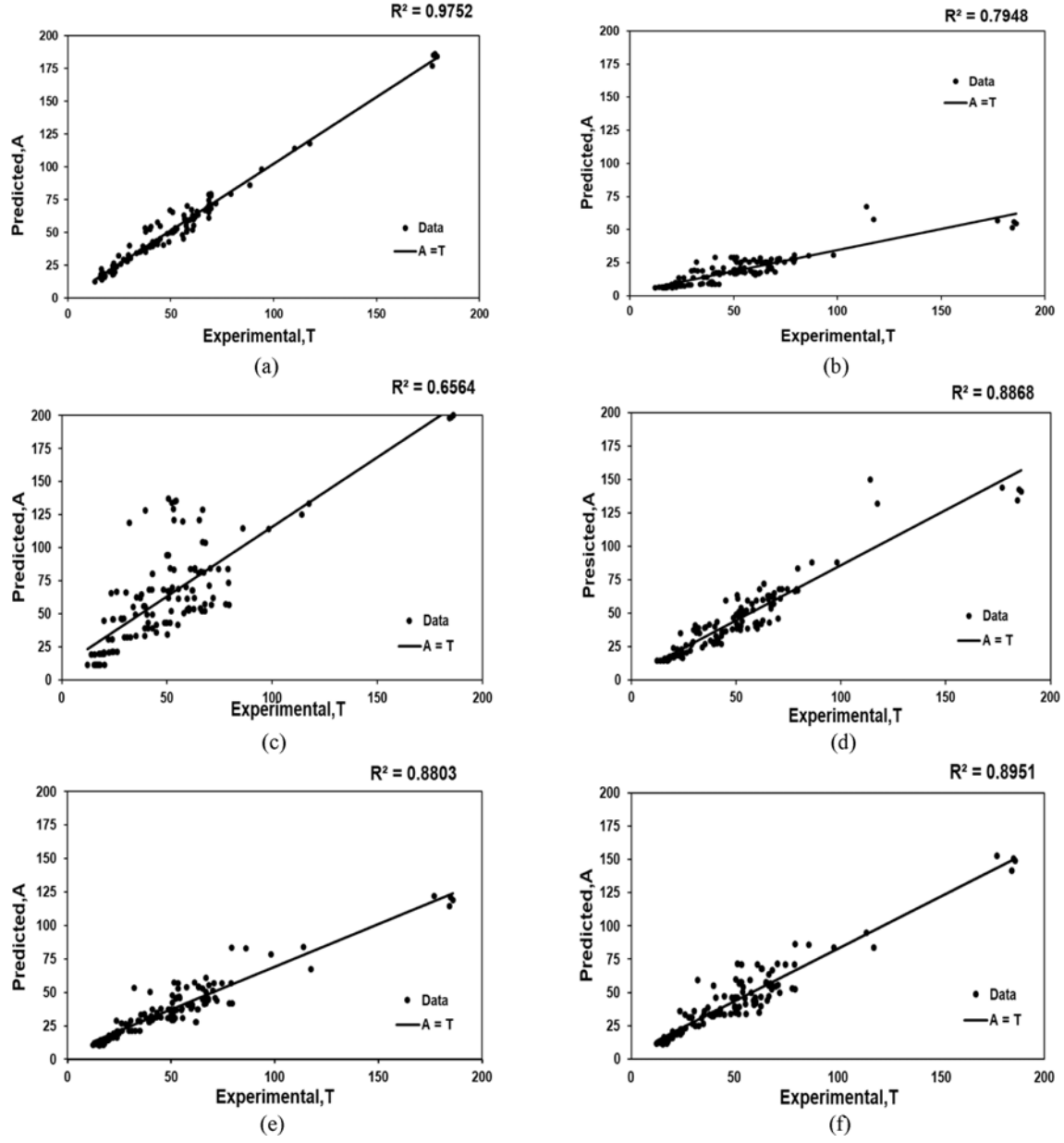

Fig. 10. Predicted Results versus Experimental Results: (a) QMESSA-BPNN, (b) ACI 440.2R, (c) AS 5100.8, (d) Shear Model, (e) TR 55, (f) Fib Bulletin 14

Table 4. Statistical Results of Each Model

	ACI 440.2R (2017)	AS 5100.8 (2017)	Fib Bulletin 14 (2001, Eq. 34)	TR 55 (2012, Eq. 37)	Shear Based Model (El-Sayed et al., 2021)	QMESSA-BPNN
R^2	0.7948	0.6564	0.8951	0.8803	0.8868	0.9752
STD	0.67	0.33	0.21	0.25	0.20	0.12
CV (%)	24.4	36.2	18.1	18.6	17.7	11.62
C (%)	100	35.94	79.7	94.5	54	14.1
N-C (%)	-	64.06	20.3	5.5	46	85.9

steel area; E_{frp} and A_{frp} are external elasticity modulus, FRP area respectively; b represents the beam width, d denotes the effective depth of tension steel, and h is the total depth of the beam.

ACI 440.2R code sets a maximum threshold for factored shear force at end point of the plate to mitigate the debonding risk at plate end.

$$V_{db,end} < 0.67 V_c , \tag{27}$$

where V_c is the beam sections concrete shear strength as established by the ACI 318 code (Wight et al., 2010; 440, 2017).

The approach taken in the AS 5100.8 is identical to the methodology found in the Concrete Society (TR 55) from 2012 and ACI 440.2R. This involves suggesting a maximum threshold for the shear force that is exerted at the region of plate end:

$$V_{dv,end} < 0.67 V_u , \tag{28}$$

where V_u is theoretical shear strength (V_u) for the beam section, which is calculated from AS 5100.5 standard (Standards Australia, 2017).

The Concrete Society Technical Report 55 (TR55) from 2012 suggests a maximum threshold considering shear force applied at plate terminating region to prevent PE debonding.

$$V_{db,end} < 0.67 V_{Rd} , \tag{29}$$

where V_{Rd} is beams shear strength, and is determined following the guidelines outlined in Eurocode 2 at Section 6.2 (European Committee for Standardization, 2004).

The concept introduced by Blaschko in 1997, as outlined in fib Bulletin 14 from 2001, relies on shear strength of concrete within the beam. The approach follows, prevention of PE debonding involves limiting the shear force exerted at the PE region to the beam shear cracking strength, as expressed in the following manner:

$$V_{db,end} < f_{ck}^{1/3} bd , \tag{30}$$

where represents the concrete compressive strength (characteristic), which is determined from Eurocode 2 (European Committee for Standardization, 2004).

Figure 10 displays the calculated values obtained from the code models, empirical shear-based model and the predicted value generated by QMESSA-BPNN model. 128 sets of experimental data have been utilized for making the prediction comparison among the model, codes and shear-based model. It is evident from the figure that the code-based model calculations exhibit a relatively discrete distribution, whereas QMESSA-BPNN outperforms ACI, TR55, AS 5100.8, Fib Bulletin and empirical shear-based model in terms of model fit and accuracy. The coefficient of determination (R^2) of QMESSA-BPNN model is 97.5% indicating a low dispersion of data set and high accountability capacity of variance by the prediction model.

Furthermore, Table 4 provides a thorough examination of the predictive precision and dependability of the model formulated in this research and comparison with national codes. The coefficient of variation for all the code models exceeds 18% whereas it is 17.7% in the empirical shear-based model.

Consequently, application in practice is difficult due to high variance. However, QMESSA-BPNN model demonstrates a lower coefficient of variation at only 11.62%. In comparison to the code models, QMESSA-BPNN model exhibits significant reduced variability. Notably, the ACI, TR55, AS 5100.8, Fib Bulletin code models as well as the shear model are highly conservative. Approximately 100%, 94.5%, 35.94%, 79.7%, and 54% of all specimens have significantly overestimated predicted values according to these models. On the other hand, the QMESSA-BPNN model significantly reduced this conservativeness with a value of 14.1% indicating the effectiveness in prediction accuracy.

7. Correlation Analysis of Parameters

The impact of various parameters on the debonding load can be determined through the weights that connect the neurons in each layer. The connection weights play a significant part in neural network as they determine the efficacy of the model output by creating a nonlinear relationship between input parameters and target output. The input layer is made up of neurons X1 to X13 (each neuron is for each parameter), while the hidden layer consists of neurons H1 to H10, and the output layer comprises of only one neuron, Y. Tables 5 and 6 shows the connection weights of interlayer neurons. These connection weights are taken from neural network architecture modelled in MATLAB.

The degree of influence of the X^{th} parameter on the debonding load, is calculated using Eq. (31).

$$P_x = \sum_{i=1}^{10} w_{xi} \times h_i , \tag{31}$$

where w_{xi} is the connection weight between X^{th} parameter and the i-th implied layer; and h_i is the connection weight between the

Table 5. Connection Weights of Input Layer and Hidden Layer

Column1	X1	X2	X3	X4	X5	X6	X7	X8	X9	X10	X11	X12	X13
H1	-2.09	1.99	-1.97	-1.97	-1.64	-1.94	-2.02	-1.92	2.03	-1.94	-2.13	1.92	-2.09
H2	2.09	1.52	0.66	2.96	-1.61	1.28	-3.00	-1.33	0.18	2.11	2.94	-2.21	1.99
H3	1.97	-1.98	2.01	-2.07	-2.02	-1.85	1.99	1.94	-2.02	-2.02	1.97	2.03	2.06
H4	-1.68	-1.75	-1.87	2.28	-1.88	2.13	-1.99	-1.68	-2.26	1.89	2.31	2.19	2.14
H5	1.94	-1.29	-2.49	-0.05	-2.09	2.19	-2.16	-1.99	-1.88	2.34	1.95	-2.20	-2.20
H6	-2.03	2.07	-1.33	-0.63	4.75	-3.32	0.94	-1.87	2.93	2.00	-0.61	-1.90	1.41
H7	-2.67	-1.64	-2.15	-2.14	2.34	0.60	-1.79	-1.83	-0.96	1.44	-2.12	-2.09	2.06
H8	1.98	1.17	-1.98	2.01	-1.37	2.02	1.80	2.02	-0.07	-1.99	2.02	-2.01	1.73
H9	1.31	1.41	1.27	-1.52	1.71	1.95	-1.15	-2.39	0.92	-1.97	0.58	2.34	0.99
H10	-0.59	-0.99	2.04	1.26	1.69	-2.49	-1.21	1.63	1.40	-0.83	-0.33	-0.32	2.34

Table 6. Connection Weights of Hidden Layer and Output Layer

Column1	H1	H2	H3	H4	H5	H6	H7	H8	H9	H10
Y	-6.25	5.13	2.05	-3.49	9.16	-5.39	2.42	-0.21	7.16	-5.43

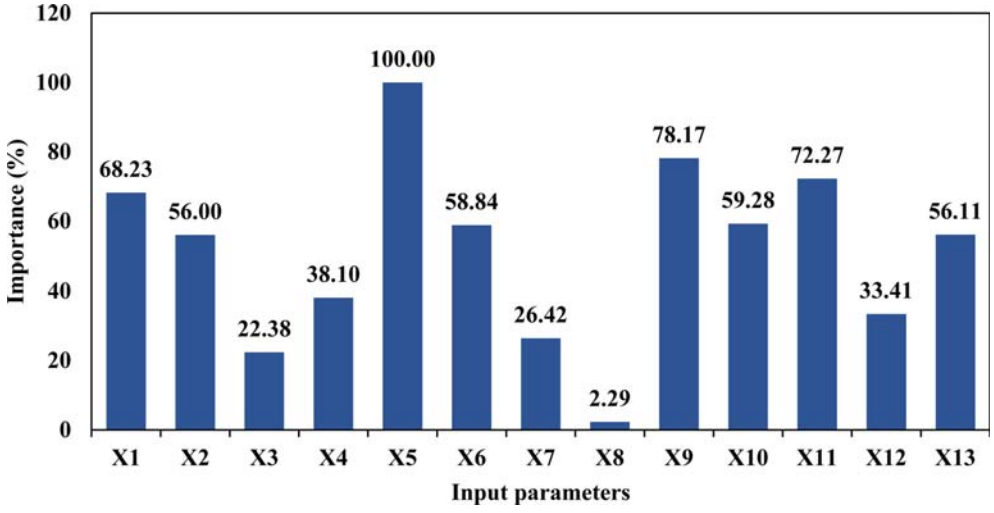

Fig. 11. Importance of Each Parameter

i implied layer and the output layer, respectively.

To get the importance of each parameter on PE debonding, the values were calculated using Eq. (31). After normalizing, the plot is shown in Fig. 11.

The graph in Fig. 11 illustrates the significance of different parameters in the proposed model, with input parameters ranging from X1 to X13 on the X-axis and the corresponding percentage contribution on the Y-axis. The most crucial parameter, X5, which represents the shear reinforcement in concrete ρ_{sv}, has the highest importance of 100%. The next important parameter is X9, which is the yield strength of steel f_y with an importance of 78.17%. Afterwards, X11, representing the thickness of FRP (t_{frp}), with an importance of 72.27%. On the other hand, the parameter X8 represents the variable L_{up}, which has the least impact on the model with an importance of only 2.29%. As can be seen from Fig. 11, the order for the importance of each parameter can be demonstrated as following:

$$\text{X5}(\rho_{sv}) > \text{X9}(f_y) > \text{X11}(t_{frp}) > \text{X1}(b) > \text{X10}(f_{fu}) > \text{X6}(E_{frp}) > \text{X13}(a) > \text{X2}(d) > \text{X4}(f_{yv}) > \text{X12}(L) > \text{X7}(b_{frp}) > \text{X3}((f_c')) > \text{X8}(L_{up});$$

This graph effectively illustrates the significance and relative contributions of various parameters in plate end debonding failure, aiding decision-making in the design process. Shear reinforcement emerges as a crucial factor in mitigating debonding in FRP-strengthened RC beams. Additionally, the model highlights the often-overlooked influence of FRP material and geometric properties, such as thickness and ultimate strength, on debonding occurrence. The intricate non-linear relationship in the model comprehensively considers all governing parameters, emphasizing the importance of accounting for these factors in FRP system design to prevent premature failures like plate end debonding.

8. Conclusions

This study presents a predictive model for debonding at the plate end region in FRP-strengthened RC beams in flexure. QMESSA optimized BPNN model demonstrates effective and accurate forecasting of debonding loads and is evaluated against several codes. The following conclusions can be drawn:

1. The QMESSA-BPNN model gives the best prediction results compared to the BPNN model. The BPNN model faces overfitting issues, with a regression value of 0.997 in training, 0.977 in validation, but 0.816 in testing. On the other hand, the QMESSA optimized BPNN model solved this overfitting problem, with both the regression value of validation and testing dataset equal to 0.99. This indicates the generalization capability and robustness of the QMESSA-BPNN model.
2. QMESSA-BPNN model significantly solved the shortcomings (convergence speed, getting out of local minima, balancing in exploration and exploitation ability of SSA) in SSA-BPNN model by an increased regression value in test dataset from 0.96 to 0.99.
3. In the parametric study of QMESSA-BPNN model, the shear reinforcement ratio was identified as the most influential factor affecting plate end debonding capacity. High reinforcement ratio enhances the shear capacity, consequently prevents debonding. Notably, factors like steel yield strength, thickness, modulus of elasticity, and FRP ultimate strength also contribute significantly to debonding load.
4. The coefficient of determination (R^2) of QMESSA-BPNN model is 97.5% indicating a low dispersion of data set and high accountability capacity of variance by the prediction model. Indicating that it optimally utilizes the strength of FRP-strengthened RC beams. This contrasts with the more conservative nature of ACI and other codes.
5. Unlike existing code provisions, the QMESSA-BPNN model considers crucial FRP properties in predicting debonding capacity. Its ability to capture complex non-linear debonding parameters suggests its potential as a superior alternative for code implementation.
6. QMESSA-BPNN model experiences some optimization issues due to complex neural network architecture, limited data, and extreme outliers. Noise in the data leads to poor prediction accuracy.
7. Data skewness and outliers' removal can be resolved by governing data pre-processing techniques, and better generalization capability of model can be achieved by increasing the dataset size.

Acknowledgments

The authors are grateful for the financial support towards this research by the Department of Civil Engineering of Chittagong University of Engineering and Technology.

Nomenclature

a	Shear span of beam
b	Beam width
b_{frp}	FRP width
BPNN	Back Propagation Neural Network
CCS	Concrete Cover Separation
d	Depth of beam
E_{frp}	Modulus of elasticity of FRP
f_c'	Concrete compressive strength
f_{fu}	Ultimate strength of FRP
FRP	Fiber Reinforced polymer
f_y	Yield strength of steel reinforcement
f_{yv}	Shear reinforcement
IC	Intermediate Crack
L	Clear span of beam
LM	Levenberg Marquardt algorithm in BPNN
L_{up}	FRP curtailment length
NN	Neural Network
PE	Plate End
$P_{u,exp}$	Debonding failure load of FRP
QMESSA	Quantum-computations and Multi-Strategy enhanced Sparrow Search Algorithm
RC	Reinforced Concrete
t_{frp}	Thickness of FRP
ρ_{sv}	Shear reinforcement ratio

ORCID

Md. Ismail Monsury https://orcid.org/0009-0001-5078-5534
Nusrat Hoque https://orcid.org/0000-0002-6912-2570
Hasnat Rahman https://orcid.org/0009-0003-4630-6291

References

440, C (2017) Aci 440.2R-17. In American Concrete Institute

Abuodeh OR, Abdalla JA, Hawileh RA (2020) Prediction of shear strength and behavior of RC beams strengthened with externally bonded FRP sheets using machine learning techniques. *Composite Structures* 234:111698, DOI: 10.1016/j.compstruct.2019.111698

Al-Saawani MA, Al-Negheimish AI, El-Sayed AK, Alhozaimy AM (2022) Finite element modeling of debonding failures in FRP-strengthened concrete beams using cohesive zone model. *Polymers* 14(9):1889, DOI: 10.3390/polym14091889

Al-Saawani MA, El-Sayed AK, Al-Negheimish AI (2015) Effect of basic design parameters on IC debonding of CFRP-strengthened shallow RC beams. *Journal of Reinforced Plastics and Composites* 34(18):1526-1539, DOI: 10.1177/0731684415593816

Al-Saawani MA, El-Sayed AK, Al-Negheimish AI (2023) Inclined FRP U-Wrap anchorage for preventing concrete cover separation in FRP strengthened RC beams. *Arabian Journal for Science and Engineering* 48(4):4879-4892, DOI: 10.1007/s13369-022-07186-6

Aram MR, Czaderski C, Motavalli M (2008) Debonding failure modes of flexural FRP-strengthened RC beams. *Composites Part B: Engineering* 39(5):826-841, DOI: 10.1016/j.compositesb.2007.10.006

Bianchini M, Gori M, Maggini M (1994) On the problem of local

minima in recurrent neural networks. *Journals & Magazines* 5(2)

Biscaia H (2001) Concrete beams strengthened with externally bonded FRP Plates. *Journal of Composites for Construction* 5(1), DOI: 10.1061/(ASCE)1090-0268(2001)5:1(44)

Chen JF, Teng JG (2001) Anchorage strength models for FRP and steel plates bonded to concrete. *Journal of Structural Engineering* 127(7): 784-791, DOI: 10.1061/(asce)0733-9445(2001)127:7(784)

Chen JF, Teng JG (2003) Shear capacity of FRP-strengthened RC beams: FRP debonding. *Construction and Building Materials* 17(1):27-41, DOI: 10.1016/S0950-0618(02)00091-0

Choi B, Lee JH, Kim DH (2008) Solving local minima problem with large number of hidden nodes on two-layered feed-forward artificial neural networks. *Neurocomputing* 71(16-18):3640-3643, DOI: 10.1016/j.neucom.2008.04.004

Deng ZC (2001) Flexural strengthening of reinforced concrete beams with externally bonded composite laminates. *Zhongguo Gonglu Xuebao/China Journal of Highway and Transport* 14(2):45

El-Sayed AK, Al-Saawani MA, Al-Negheimish AI (2021) Empirical shear based model for predicting plate end debonding in FRP strengthened RC beams. *Journal of Civil Engineering and Management* 27(2):117-138, DOI: 10.3846/jcem.2021.14304

Eslami A, Shayegh HR, Moghavem A, Ronagh HR (2019) Experimental and analytical investigations of a novel end anchorage for CFRP flexural retrofits. *Composites Part B: Engineering* 176(February): 107309, DOI: 10.1016/j.compositesb.2019.107309

European Committee for Standardization (2004) EN 1992-1-1: Eurocode 2: Design of concrete structures - Part 1-1: General rules and rules for buildings. Brussels: European Committee for Standardization

Hollaway LC (2010) A review of the present and future utilisation of FRP composites in the civil infrastructure with reference to their important in-service properties. *Construction and Building Materials* 24(12):2419-2445, DOI: 10.1016/j.conbuildmat.2010.04.062

International Federation for Structural Concrete (fib) (2001) Externally bonded FRP reinforcement for RC structures (fib Bulletin 14). fib, Lausanne, Switzerland, ISBN 978-2-88394-054-3, DOI: 10.35789/fib.BULL.0014

Jansze W (1997) Strengthening of reinforced concrete members in bending by externally bonded steel plates: Design for beam shear and plate anchorage [Delft University Press]. http://resolver.tudelft.nl/uuid:ca3ae758-5c6d-4da9-8866-26340c49c9e6

John OD (1992) Reinforced concrete beams with plates glued to their soffits. *Journal of Structural Engineering* 118(8):2023-2038, DOI: 10.1061/(ASCE)0733-9445(1992)118:8(2023)

Köroglu MA (2019) Artificial neural network for predicting the flexural bond strength of FRP bars in concrete. *Science and Engineering of Composite Materials* 26(1):12-29, DOI: 10.1515/secm-2017-0155

Kotynia R, Oller E, Marí A, Kaszubska M (2021) Efficiency of shear strengthening of RC beams with externally bonded FRP materials – State-of-the-art in the experimental tests. *Composite Structures* 267(September 2020):113891, DOI: 10.1016/j.compstruct.2021.113891

Lau KT, Dutta PK, Zhou LM, Hui D (2001) Mechanics of bonds in an FRP bonded concrete beam. *Composites Part B: Engineering* 32(6):491-502, DOI: 10.1016/S1359-8368(01)00032-4

Li G, Hu T, Bai D (2021) BP Neural network improved by sparrow search algorithm in predicting debonding strain of FRP-Strengthened RC Beams. *Advances in Civil Engineering*, 2021, DOI: 10.1155/2021/9979028

Ma Y, Li L, Yin Z, Chai A, Li M, Bi Z (2021) Research and application of network status prediction based on BP neural network for intelligent production line. *Procedia Computer Science* 183(2018):189-196, DOI: 10.1016/j.procs.2021.02.049

Narayanamurthy V, Chen JF, Cairns J, Oehlers DJ (2012) Plate end debonding in the constant bending moment zone of plated beams. *Composites Part B: Engineering* 43(8):3361-3373, DOI: 10.1016/j.compositesb.2012.01.060

Sen R (2015) Developments in the durability of FRP-concrete bond. *Construction and Building Materials* 78:112-125, DOI: 10.1016/j.conbuildmat.2014.12.106

Smith ST, Teng JG (2002) FRP-strengthened RC beams. II: Assessment of debonding strength models. *Engineering Structures* 24(4):397-417, DOI: 10.1016/S0141-0296(01)00106-7

Standards Australia (2017) Bridge design, Part 8: Rehabilitation and strengthening of existing bridges. Standards Australia, Sydney, Australia, https://store.standards.org.au/product/as-5100-8-2017

The Concrete Society (2012) Design guidance for strengthening concrete structures using fibre composite materials (Technical Report 55). The Concrete Society, UK

Wight JK, Barth FG, Becker MA (2010) ACI Committee 318, "Building Code requirements for structural concrete (ACI 318-10) and commentary (ACI 318R-10)." *American Concrete Institute, Farmington Hills, MI* 2003:430

Wu R, Huang H, Wei J, Ma C, Zhu Y, Chen Y, Fan Q (2023) An improved sparrow search algorithm based on quantum computations and multi-strategy enhancement. *Expert Systems with Applications* 215(December), DOI: 10.1016/j.eswa.2022.119421

Xue J, Shen B (2020) A novel swarm intelligence optimization approach: Sparrow search algorithm. *Systems Science and Control Engineering* 8(1):22-34, DOI: 10.1080/21642583.2019.1708830

Yu S, Zhu K, Diao F (2008) A dynamic all parameters adaptive BP neural networks model and its application on oil reservoir prediction. *Applied Mathematics and Computation* 195(1):66-75, DOI: 10.1016/j.amc.2007.04.088